Research Square

Preprints are preliminary reports that have not undergone peer review.
They should not be considered conclusive, used to inform clinical practice,
or referenced by the media as validated information.

Design and Evaluation of Boron-Containing Polymer Scaffolds Developed with Rat Mesenchymal Stem Cells for Bone Tissue Engineering Applications

Günnaz Çapan
Istanbul University
Erdi Buluş
Istanbul Arel University
Gürcan Albeniz
Gebze Fatih State Hospital
Bukem Tanören
Acıbadem University
Leyla Türker Şener
Istanbul University
Işıl Albeniz
ialbeniz@istanbul.edu.tr

Istanbul University

Research Article

Keywords: electrospinning, hexagonal boron nitride (hBN), nanofibrous scaffold, mesenchymal stem cells, bone tissue engineering

Posted Date: November 27th, 2026

DOI: https://doi.org/10.21203/rs.3.rs-11785145/v1

License: This work is licensed under a Creative Commons Attribution 4.0 International License.
Read Full License

Additional Declarations: No competing interests reported.

Design and Evaluation of Boron-Containing Polymer Scaffolds Developed with Rat Mesenchymal Stem Cells for Bone Tissue Engineering Applications

Günnaz Çapan[1], Erdi Buluş[2], Gürcan Albeniz[3,4], Bukem Tanören[5], Leyla Türker Şener[1], Işıl Albeniz[1]

[1] Istanbul Univerity Faculty of Medicine, Department of Biophysics, Istanbul University, Fatih 34093, Türkiye

[2] ArelPOTKAM (Polymer Technologies and Composite Application and Research Center), Istanbul Arel University, Istanbul 34537, Türkiye

[3] Department of General Surgery, Gebze Fatih State Hospital, Kocaeli, Türkiye

[4] Department of Molecular Medicine, Institute of Health Sciences, Istanbul University, Istanbul, Türkiye

[5] Acibadem University, Istanbul, Türkiye

Corresponding Author

Işıl Albeniz

ialbeniz@istanbul.edu.tr

ABSTRACT

Bone fractures and critical-sized defects remain major challenges in regenerative medicine, highlighting the need for biomaterial scaffolds that support cellular activity and osteogenic maturation. In this study, electrospin poly(ε-caprolactone) (PCL)–hydroxyapatite (HA) nanofiber scaffolds incorporating different concentrations of hexagonal boron nitride (hBN; 0.05%, 0.5%, and 2.5%) were fabricated to investigate the influence of hBN loading on scaffold physicochemical properties, mechanical behavior, and cellular responses. Fourier-transform infrared spectroscopy (FTIR) and scanning electron microscopy (SEM) were used to characterize the scaffolds, while tensile testing was performed to evaluate their mechanical properties. FTIR analysis supported the incorporation of HA and hBN, whereas SEM revealed non-linear variations in fiber diameter with increasing hBN content. Mechanical testing revealed a progressive decrease in maximum tensile stress with increasing hBN concentration, from 3.074 MPa in the hBN-free scaffold to 0.480 MPa in the scaffold containing 2.5% hBN. Biological evaluation using rat bone marrow-derived mesenchymal stem cells (rBM-MSCs) demonstrated sustained metabolic activity across all scaffold formulations at 24 hours and day 5. Confocal fluorescence imaging revealed differences in cellular organization and fluorescence intensity depending on hBN concentration. Alizarin Red S analysis demonstrated concentration- and time-dependent increases in mineral deposition, with the 2.5% hBN scaffold exhibiting the highest mineralization response across the evaluated time points. Collectively, these findings suggest that hBN incorporation differentially influences scaffold mechanical properties and osteogenic responses, highlighting the importance of balancing mechanical performance and biological functionality in the design of nanofibrous scaffolds for bone tissue engineering.

Keywords: electrospinning, hexagonal boron nitride (hBN), nanofibrous scaffold, mesenchymal stem cells, bone tissue engineering

Introduction

Bone is a vascularized and dynamic hard tissue capable of repairing minor defects. However, bone defects arising from trauma, osteoporosis, and tumors pose significant challenges for regenerative medicine [1, 2]. The primary goal in treating bone defects is to achieve rapid and spontaneous healing, and bone grafting remains one of the most widely used approaches in this process. More than two million bone grafting procedures are performed worldwide each year, making it the second most common tissue transplantation after blood transfusion [3]. Currently, allografts and autografts are the two main strategies used in maxillofacial and orthopedic surgery to repair or replace damaged bone tissue [1]. Nevertheless, conventional autologous and allogeneic grafts often fail to provide satisfactory outcomes in severe fractures or pathological conditions including critical-sized defects caused by osteoporosis, malformations, or cancer due to limitations such as low cell viability and insufficient graft vascularization [3, 4]. Metallic implants such as stainless steel and titanium are widely used to treat bone defects; however, their limited lifespan and excessive stiffness reduce physiological load-sharing and can lead to bone resorption and long-term structural weakening. Such structural and biomechanical limitations have encouraged the development of innovative and biocompatible strategies in tissue engineering and biomaterials research [5, 6]. Bone tissue engineering (BTE) aims to restore the structure and function of damaged bone by integrating materials science, engineering principles, biology, and stem cell technologies. A central component of this approach is the development of osteoconductive scaffolds that support cellular attachment, proliferation, and osteogenic activity while providing an appropriate environment for tissue formation and vascularization [1, 7]. Electrospin nanofibers have emerged as a promising strategy for mimicking the mineralized organic structure of native bone. Hybrid composites composed of inorganic materials and electrospin fibers are considered effective at replicating the extracellular matrix (ECM) environment and thus promoting favorable outcomes in bone

defect healing [8, 9]. These biomimetic materials can be used as hybrid composites that facilitate nutrients and oxygen transport while maintaining desirable biomechanical properties [10]. Among polyester-based polymers, polycaprolactone (PCL) is widely preferred in tissue engineering due to its biodegradability and biocompatibility. Its ester linkages render it susceptible to hydrolytic degradation, allowing gradual resorption under physiological conditions and making it attractive for bone regeneration. Despite possessing a semi-crystalline architecture, marked hydrophobicity, and a relatively low melting temperature, PCL inherently lacks osteoinductive capability; therefore, further modifications are required to enhance its biological functionality [11, 12]. To address the limitations of polymeric scaffolds in terms of mechanical stability, cell adhesion, and osteogenic stimulation, recent research has focused on the development of composite structures incorporating functional additives. Carbon-based nanomaterials (e.g., graphene oxide, carbon nanotubes), piezoelectric ceramics (e.g., barium titanate, zinc oxide), and calcium phosphate based compounds have been widely explored as reinforcing agents that enhance the biological and structural performance of polymer matrices [13]. Among these, calcium phosphate phases have attracted considerable attention due to their structural and chemical resemblance to native bone. Incorporation of calcium phosphate compounds into polymeric systems not only improves mechanical strength but also enhances cellular interaction and osteogenic differentiation [14]. Hydroxyapatite (HA), which constitutes the mineral phase of bone, is the most prominent of these biomolecules. By increasing local Ca+2 concentration, HA promotes osteoblast proliferation and stimulates the growth and differentiation of mesenchymal stem cells (MSCs). Its nonimmunogenic nature, high biocompatibility, biological activity, and osteoconductive properties have made HA a widely used material in bone repair and regeneration. Various HA based materials including pure HA, ion doped HA, and HA/polymer composites have been developed to date. However, HA still presents drawbacks such as brittleness and a tendency to aggregate. Therefore, the development

of HA based composite systems with improved mechanical stability and biological performance remains a significant research focus in bone tissue engineering [11, 15, 16].

Boron is a trace element playing vital roles in physiological processes such as bone growth, immune regulation, and hormone metabolism. It contributes to brain development, inflammatory modulation, and tooth bone formation. Multiple in vitro studies have shown that boron-containing systems enhance adhesion, proliferation, and mineralization in osteoblasts and MSCs [17-19]. Boron has also been shown to activate osteogenic differentiation by upregulating bone-related matrix proteins such as osteocalcin, osteopontin and Runx2. Both oral supplementation and local delivery have demonstrated favorable effects on bone health [20, 21]. Furthermore, boron regulates vitamin D metabolism, increases calcium and magnesium absorption, and exerts estrogen-like effects that may reduce postmenopausal osteoporosis risk [22, 23]. Its anti-inflammatory effects, including reductions in TNF-α and IL-6 and increases in superoxide dismutase (SOD) and glutathione peroxidase activities, have also been reported [24, 25]. However, the biological activity of boron is dose dependent. Excessive intake can cause gastrointestinal irritation, dizziness, and liver dysfunction; thus, maintaining biocompatible concentration ranges is essential. The World Health Organization (WHO) defines a safe daily intake for healthy adults as 1–13 mg/day, whereas the European Food Safety Authority (EFSA) sets the upper tolerable intake at 0.16–0.4 mg B/kg/day (approximately 12–30 mg/day) [26, 27]. Therefore, the multifunctional biological effects of boron supporting osteogenic mechanisms at the cellular level and regulating bone metabolism systemically make it an attractive candidate for the development of biomaterial systems in tissue engineering. Nevertheless, boron's dose-dependent activity underscores the importance of identifying optimal, biocompatible concentration ranges. The choice of cellular source in bone regeneration is as critical as scaffold design. Biocompatible scaffolds must be optimized to support cell adhesion, proliferation, and long-term viability. Microporous scaffolds, with their high surface-

to-volume ratio and low density, facilitate cell suspension and offer potential advantages in bioreactor applications. Mesenchymal stem cells (MSCs), with remarkable plasticity, high proliferative capacity, and multipotent differentiation potential including osteoblast lineage have emerged as ideal biological tools for tissue engineering and autologous bone transplantation [28-30]. The aim of this study is to synergistically combine the excellent processability and mechanical strength of polycaprolactone (PCL) with the osteoinductive properties of hydroxyapatite (HA), while integrating hexagonal boron nitride (h-BN) at biocompatible concentrations. The goal is to fabricate porous, mechanically optimized, and biologically active scaffolds that maximize the adhesion, proliferation, and osteogenic differentiation of mesenchymal stem cells isolated from rat bone marrow.

MATERIALS AND METHODS

Chemical Reagents

All chemicals and reagents used in this study were of analytical grade and purchased from commercial suppliers. The following materials were used: Complete RPMI 1640 medium (BioWhittaker), high-glucose Dulbecco's Modified Eagle Medium (DMEM; Gibco), fetal bovine serum (FBS; Gibco), penicillin–streptomycin (HyClone), phosphate-buffered saline (PBS; Invitrogen), osteogenic differentiation kit (Gibco), 3-(4,5-dimethylthiazol-2-yl)-2,5-diphenyltetrazolium bromide (MTT; Sigma-Aldrich), trypsin (Sigma-Aldrich), MEM non-essential amino acids solution (Gibco), ethanol (Sigma-Aldrich), formaldehyde (Sigma-Aldrich), Alexa Fluor® 488 phalloidin (Invitrogen), dimethyl sulfoxide (DMSO), Alizarin Red S (ARS; Sigma-Aldrich), Ficoll® 400 reagent (Sigma-Aldrich), poly(ε-caprolactone) (PCL; M_w=80 000 g/mol, 97% purity; Sigma-Aldrich), N,N-dimethylformamide (DMF; Sigma-Aldrich), chloroform (CHCl_3; Sigma-Aldrich), hydroxyapatite (HA; Sigma-Aldrich), and hexagonal boron nitride (hBN; BORTEK Bor Teknolojileri ve Mekatronik San. Tic. A.Ş.). All materials were used without further purification. The equipment used in this study included a refrigerated centrifuge (Hettich Universal 32), a microplate reader (BioTek Epoch), a confocal laser scanning microscope (Zeiss LSM 700), and a light microscope (Olympus).

Preparation of Scaffold Solution

For the preparation of polymer scaffolds, poly(ε-caprolactone) (PCL) pellets were dissolved in appropriate solvents to obtain a stock solution. The solution containing 10 wt% PCL in chloroform and N,N-dimethylformamide (DMF) at a 3:2 ratio was homogenized using a heated magnetic stirrer. After complete dissolution of PCL, the heating was discontinued and the solution was further stirred for 1 h to ensure homogeneity. Subsequently, 10 mL of the stock solution was aliquoted, and 8 wt% hydroxyapatite (HA) was added to each sample. Polymer/bioceramic composite solutions with different compositions were then prepared by

incorporating hexagonal boron nitride (hBN) at concentrations of 0.05%, 0.5%, and 2.5%, respectively. Each mixture was homogenized at 0°C for 2 h using a magnetic stirrer to ensure uniform dispersion of HA and hBN particles [31, 32].

Production of Scaffold

PCL/HA/hBN biocomposite solutions prepared for nanofiber production by electrospinning were taken into 10 mL syringes and placed in the electrospinning device. During the electrospinning process, the distance between the needle tip and the collector was set to 10 cm, the flow rate was set to 0.100 mL/h, and the applied voltage was in the range of 13–15 kV. Under the influence of the high voltage, the polymer solutions were drawn from the needle tip and directed toward the collector surface at room temperature, and scaffolds were formed by the deposition of nanofibers on an oil paper–coated surface.

Structural Analysis of Scaffolds

Fourier Transform Infrared Spectroscopy (FTIR) analysis was performed to investigate the structural characteristics of electrospin poly(ε-caprolactone)/hydroxyapatite (PCL/HA) biocomposite scaffolds containing different concentrations of hexagonal boron nitride (hBN). FTIR spectra were acquired in the wavenumber range of 400–4400 cm^{-1} using a JASCO FT/IR-6600 spectrometer in order to identify the characteristic functional groups and evaluate possible interactions between the scaffold components.

Mechanical Tests of Scaffolds

The tensile mechanical properties of the biocomposite scaffolds were evaluated using a uniaxial tensile testing method. Prior to testing, the scaffolds were cut into rectangular specimens with a width of 1 cm and a length of 5 cm. Tensile tests were performed in accordance with the ASTM D882-10 standard using a DEVOTRANS DVT UZM K3 tensile–compression testing machine. The tests were conducted under a maximum load of 500 N, a crosshead speed of 5

mm/min, and an initial grip separation of 10 mm. Each scaffold group was tested five times, and all measurements were carried out under identical experimental conditions.

Morphological Analysis of Scaffolds

Field-emission scanning electron microscopy (FEG-SEM) was used to characterize the surface morphology and fiber architecture of the biocomposite scaffolds. Prior to imaging, samples were sputter-coated with gold–palladium (Au/Pd) under an argon atmosphere for 40 s to improve surface conductivity. After coating, micrographs were acquired using a FEI Quanta FEG 450 (FEI, Quanta) equipped with high- and low-vacuum detectors at magnifications of 1500×, 3000×, 6000×, and 12000×.

Fiber diameter distribution was determined by measuring n=150 fibers for each scaffold group from randomly selected SEM micrographs. Measurements were performed using ImageJ (NIH, USA) after calibration with the corresponding scale bar. Results were presented as frequency histograms and reported as mean ± standard deviation (SD).

SEM images obtained at 3000x magnification were analyzed using ImageJ software. Following scale calibration and conversion to 8-bit grayscale, the images were thresholded (80–255) to determine the apparent two-dimensional void fraction; subsequently, the "Analyze Particles" function was employed to evaluate the pore area distribution, excluding regions that intersected with the image boundaries. The apparent two-dimensional void area fraction was calculated as the percentage of pixels corresponding to void regions relative to the total image area, following an image-based approach like that described by Marrella et al. [33].

Sterilization of Scaffolds

The biocomposite scaffolds were sterilized prior to cellular studies. The scaffolds were soaked in 70% (v/v) ethanol prepared with ultrapure water for 2 h at room temperature and then washed three times for 5 min each with sterile phosphate-buffered saline (PBS) to remove ethanol residues. After washing, the scaffolds were placed in culture dishes and sterilized under

ultraviolet (UV) light for 45 min on both surfaces. Prior to cell seeding, the scaffolds were incubated in an oven with 95% humidity and 5% CO_2 for 24 h to allow interaction with serum proteins in the medium.

Cellular Experiments

Cell Culture

Femur and tibia bones were carefully harvested from rats anesthetized with a ketamine/xylazine mixture (2:1) to ensure adequate sedation and minimize pain or distress during the procedure. All experimental protocols were approved by the Animal Ethics Committee of Bezmialem Vakif University Experimental Application and Research Center (Approval No: 2021/251). Following isolation, the bones were thoroughly washed with sterile phosphate-buffered saline (PBS) to remove residual soft tissues.

To access the bone marrow, the epiphyseal ends of the femur and tibia were aseptically excised under sterile conditions. The marrow cavities were flushed with a sterile isotonic solution using an insulin syringe, and the resulting cell suspension was collected into centrifuge tubes. The suspension was centrifuged at 1000 rpm for 5 min, and the supernatant was discarded. The cell pellet was resuspended in fresh culture medium and carefully layered onto a 1:1 Ficoll density gradient. Following centrifugation at 2500 rpm for 25 min, the mononuclear cell layer was collected from the interface and seeded into 25 cm^2 tissue culture flasks. Cells were incubated under standard culture conditions (37°C, 5% CO_2). The primary culture (P0) was maintained for three days, and medium changes were performed every 2–3 days. Upon reaching 70–80% confluence, cells were detached using trypsin–EDTA and passaged into new flasks for further expansion [34]. This protocol enabled efficient isolation and expansion of rat bone marrow derived mesenchymal stem cells (rBM-MSCs), preserving cell viability and functional properties for subsequent scaffold seeding and osteogenic differentiation studies.

MTT Assays

The cellular viability and mitochondrial activity of nanofiber scaffolds containing different concentrations of hexagonal boron nitride (hBN) (0%, 0.05%, 0.5%, and 2.5% w/v) were evaluated using the MTT assay (3-(4,5-dimethylthiazol-2-yl)-2,5-diphenyltetrazolium bromide). Sterilized scaffolds were aseptically placed into 96-well tissue culture plates, and cells were seeded at a density of 5×10^4 cells/cm^2. The cultures were maintained under standard incubation conditions (37°C, 5% CO_2). Wells containing scaffolds incubated with culture medium without cells were used as negative controls, while wells containing cells cultured without scaffolds served as positive controls.

Cell viability was assessed after 1 and 5 days of incubation. At each time point, 20 µL of MTT solution was added to each well and incubated at 37°C for 4 h. Subsequently, the resulting formazan crystals were dissolved in dimethyl sulfoxide (DMSO), and absorbance values were measured at 570 nm using a microplate reader. The absorbance intensity was considered proportional to the number of viable cells [35].

Confocal Microscope Imaging

Confocal laser scanning microscopy (CLSM) was used to evaluate cell adhesion, distribution, and morphological characteristics on the nanofiber scaffolds. Cytoskeletal organization and cell morphology were visualized by staining filamentous actin (F-actin) using Alexa Fluor® 488–conjugated phalloidin. Cells were seeded onto each scaffold at a density of 1.5×10^3 cells/cm^2 and incubated under standard culture conditions (37°C, 5% CO_2, humidified atmosphere).

Cell–scaffold interactions were examined at two time points, 1 and 5 days, representing early adhesion and subsequent cell spreading. At the designated time points, samples were fixed with 4% formaldehyde for 15 min at room temperature to preserve cellular morphology, followed by three washes with phosphate-buffered saline (PBS). The fixed samples were then incubated with Alexa Fluor® 488 phalloidin (165 nM) for 20 min at room temperature in the dark to label

F-actin filaments. After staining, excess dye was removed by washing with PBS. The stained scaffolds were examined using a confocal laser scanning microscope, and images were acquired at different magnifications to assess overall cell distribution as well as detailed cellular morphology on the scaffold surfaces.

Alizarin Red Staining

Alizarin Red S staining was performed to evaluate osteogenic differentiation and mineralized matrix formation on biocomposite scaffolds. The scaffolds were cultured in osteogenic medium prepared using a commercial differentiation kit under standard culture conditions (37°C, 5% CO_2) for 21 days. Samples were fixed with 4% formaldehyde at days 5, 10, 15, and 20, followed by staining with Alizarin Red S solution (pH 4.2) for 20 min at room temperature. Excess dye was removed by washing with distilled water.

Quantitative analysis of Alizarin Red S–positive areas was carried out using ImageJ software (NIH, USA). Images were acquired using a standard digital camera under identical conditions. For each group and time point, three independent replicates (n=3) were analyzed. RGB images were split into individual channels, and analysis was performed on the red channel. A fixed circular region of interest (ROI) covering the scaffold area was applied to all images. Thresholding was performed using identical parameters, and the percentage of Alizarin Red positive area was calculated. Results were expressed as mean ± standard deviation.

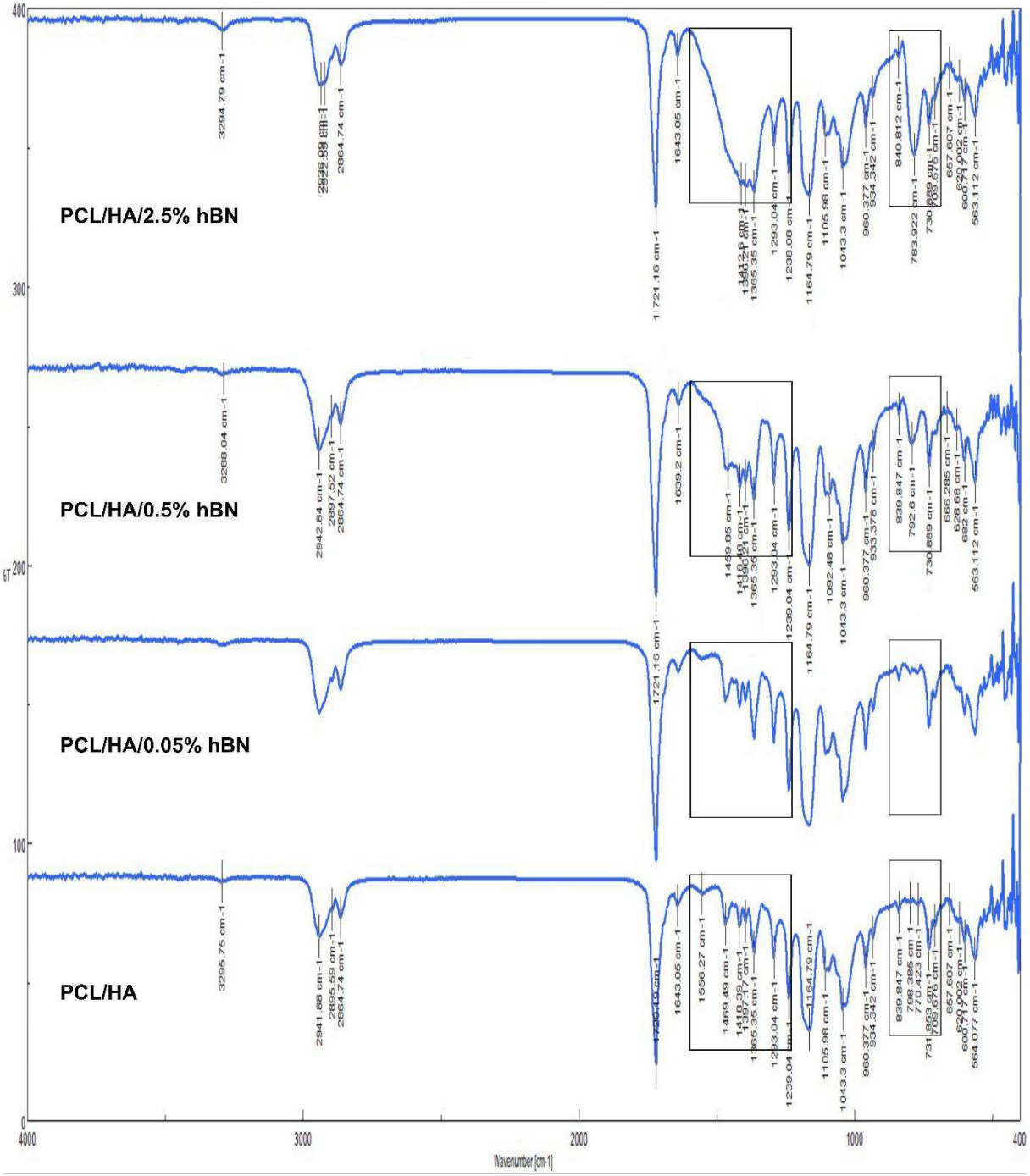
Statistical Analysis

All experimental data are presented as mean ± standard deviation (mean ± SD). All experiments were performed independently in triplicate (n=3). Statistical analyses were conducted to evaluate differences among experimental groups. One-way analysis of variance (ANOVA) was applied, followed by Tukey's post hoc multiple comparison test to determine statistically significant differences between individual groups. A p-value of less than 0.05 ($p<0.05$) was considered statistically significant. All statistical analyses and graphical visualizations were

performed using the Python programming language, utilizing appropriate scientific computing and plotting libraries to ensure accurate data processing, statistical evaluation, and high-quality graphical representation.

Cell viability was calculated according to the following equation (1):

$$\text{Cell Viability (\%)} = \frac{\text{Absorbance of treated cells}}{\text{Absorbance of control cells}} \times 100 \quad (1)$$



FTIR Results

Fourier Transform Infrared Spectroscopy (FTIR) analysis was performed to determine the chemical composition of the scaffolds and to characterize their functional groups. As shown in Figure 1, FTIR spectra of 10% PCL / 8% HA–based scaffolds containing different ratios of hexagonal boron nitride (hBN) were evaluated.

The spectra exhibited characteristic infrared absorption bands corresponding to poly(ε-caprolactone) (PCL). The asymmetric and symmetric stretching vibrations of the methylene (CH_2) groups of PCL were observed at 2942 cm^{-1} and 2864 cm^{-1}, respectively. In addition, a strong absorption band at 1721 cm^{-1} corresponding to the carbonyl (C=O) group, which is a hallmark of PCL, was detected. This band serves as an important indicator of the ester bonds in PCL and provides insight into both the amorphous and semi-crystalline phases of the polymer. The bands at 1293 cm^{-1}, attributed to C=O and C–C stretching modes, and at 1239 cm^{-1} , corresponding to asymmetric C–O–C stretching in the crystalline phase, were also clearly identified in accordance with the literature [8].

The presence of hydroxyapatite (HA) nanoparticles was confirmed by the characteristic phosphate (PO_4^{-3}) vibrational bands observed at 563, 601, 960, 1029, and 1105 cm^{-1}. Among these, the band at 960 cm^{-1} is of particular importance as it indicates the preservation of the crystalline structure of hydroxyapatite [8, 36].

Moreover, a pronounced increase in band intensity was observed in the ~780–790 cm^{-1}region with increasing hBN content. This region corresponds to the B–N–B bending vibration of hBN, and the enhancement was especially evident in samples containing 0.5% and 2.5% hBN, supporting the successful dispersion and incorporation of hBN nanoplatelets within the scaffold matrix. In addition, a secondary increase in band intensity was detected in the 730–750 cm^{-1} region, which is attributed to matrix-induced frequency shifts of the B–N–B bending mode combined with PCL backbone vibrations and phosphate-related modes of HA. In the pure PCL/HA scaffold, a small shoulder band observed around 1300–1566 cm^{-1} gradually diminished and completely disappeared with increasing hBN content [37, 38]. This behavior indicates that the incorporation of hBN restricts the local mobility of PCL chains and suppresses CH_2 bending vibrations associated with the amorphous phase of the polymer. The disappearance of this shoulder band further supports the presence of physical interactions

between hBN and the PCL matrix. FTIR results demonstrate the successful incorporation of PCL, HA, and hBN into the composite structure. The increasing hBN content contributes to matrix interactions, as evidenced by the spectral modulations observed particularly in the 1350–1500 cm^{-1} and 730–750 cm^{-1} regions.

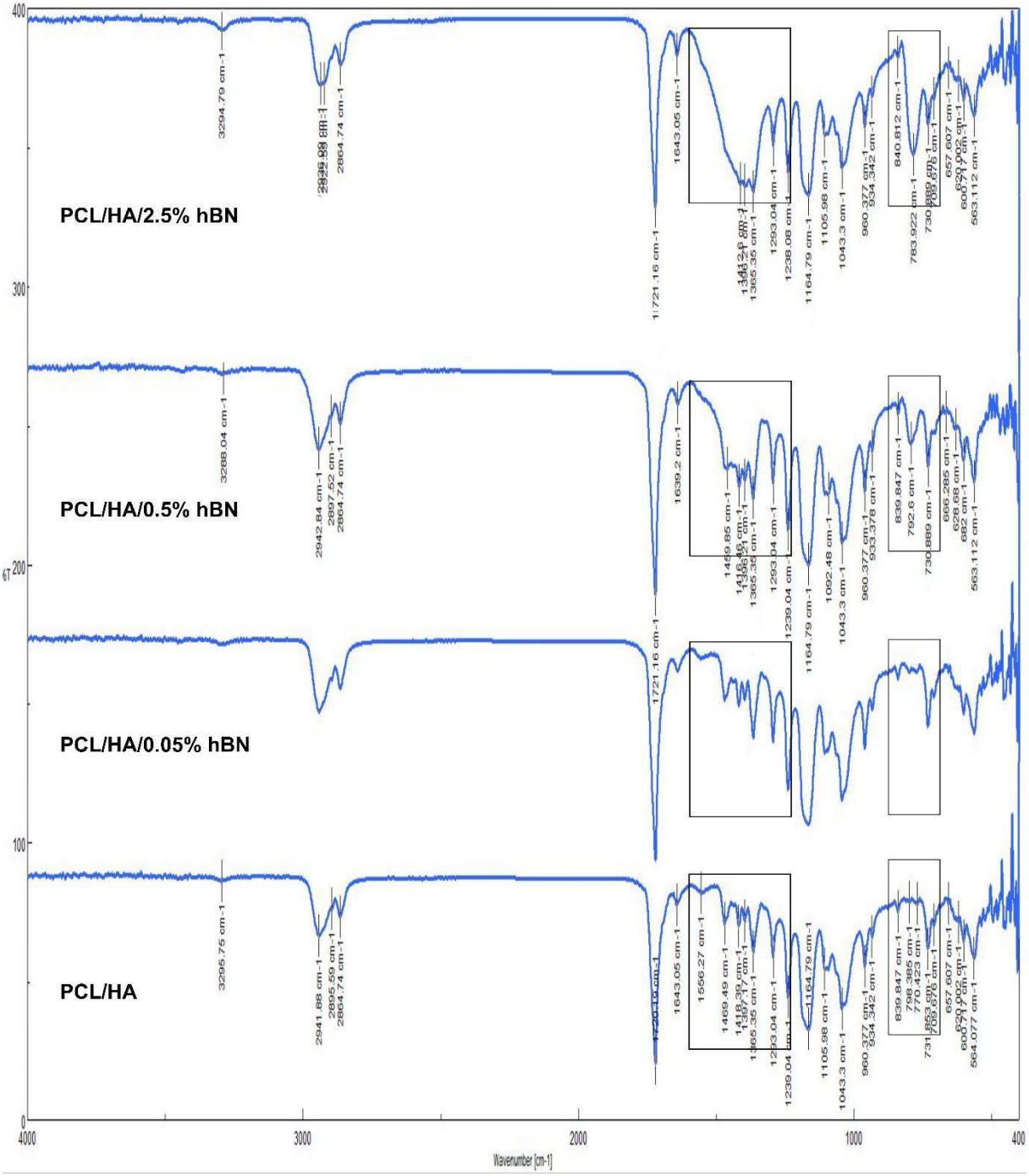


Fig. 1 Fourier Transform Infrared Spectroscopy (FTIR) spectra of PCL/HA/hBN composite scaffolds with varying hBN concentrations: 10% PCL/8% HA (control), 10% PCL/8% HA/0.05% hBN, 10% PCL/8% HA/0.5% hBN, and 10% PCL/8% HA/2.5% hBN. The x-axis represents the wavenumber (cm^{-1}), and the y-axis corresponds to absorbance intensity.

Tensile Test Results

The tensile properties of the biocomposite scaffolds were evaluated by uniaxial tensile testing in accordance with ASTM D882 standards. All samples were prepared with identical geometrical dimensions (thickness: 0.2 mm, width: 10 mm, initial cross-sectional area: 2 mm^2) to ensure consistency and comparability between groups. For each scaffold composition, tensile testing was conducted on five independent specimens ($n = 5$). The obtained mechanical parameters were expressed as mean $\pm$ standard deviation, as summarized in Table 1. Representative stress–strain curves for each composition are presented in Figure 2.

The tensile curves exhibited an initial elastic response at low extensions, followed by a progressively nonlinear deformation regime and a final failure stage characterized by a sharp decrease in stress. Differences in the overall shape and deformation range of the curves among the samples reflect composition-dependent variations in tensile behavior.

According to the tensile data, Sample 2 exhibited the highest mechanical performance among all tested specimens, reaching a maximum force (F_{max}) of 6.147 N and a corresponding maximum tensile stress (σ_{max}) of 3.074 MPa. This behavior is also clearly reflected in Figure 2, where Sample 2 attains the highest stress level and maintains its load-bearing capacity over a relatively wide extension range before fracture, indicating effective stress transfer within the composite structure. In contrast, Sample 4 demonstrated moderately high tensile strength ($F_{max} = 5.492$ N, $\sigma_{max} = 2.746$ MPa) but failed at a noticeably lower extension compared to Sample 2. The abrupt stress drop observed in its stress–extension curve suggests a more brittle fracture mechanism, which may be attributed to reduced ductility or limited energy dissipation during deformation. Samples 5 and 7 exhibited significantly lower tensile strength values, with maximum stresses of only 0.48 MPa and 0.821 MPa, respectively, indicating insufficient load transfer efficiency within these composites. Their stress–extension curves remained at low

stress levels throughout the test, reflecting premature failure under tensile loading and inadequate mechanical reinforcement of the polymer matrix.

The elongation behavior further distinguished the mechanical responses of the samples, as Sample 2 displayed the highest elongation at break, with a maximum extension ($\Delta l_{\max}$) of 3.266 mm and a corresponding strain ($\varepsilon_{\max}$) of 6.532%, demonstrating a balanced combination of strength and ductility. Although Sample 4 exhibited relatively high tensile strength, its reduced elongation at break ($\varepsilon_{\max} = 4.166\%$) confirmed the transition toward a more brittle deformation mode, which is consistent with the sharp stress drop observed in Figure 2.

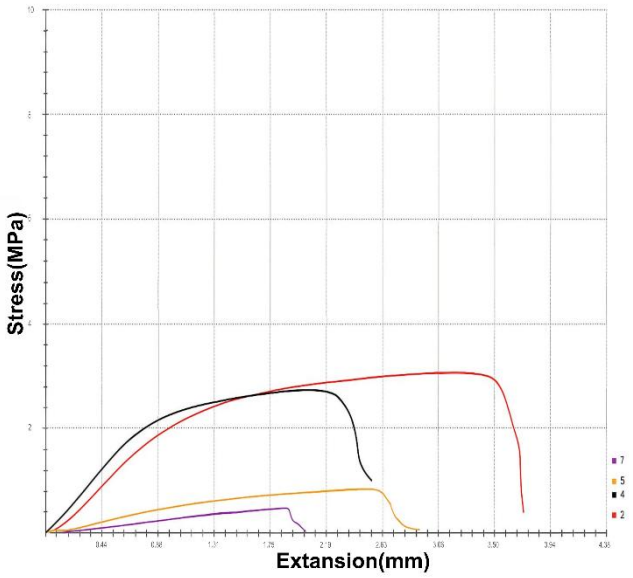


Fig. 2 Stress–strain curves of PCL/HA/hBN composite scaffolds with different compositions, illustrating the mechanical response and deformation behavior under tensile loading.

Table 1 Tensile properties of scaffolds.

Sample No.	$F_{\max}$ (N)	$\Delta l_{\max}$ (mm)	$\varepsilon_{\max}$ (%)	$\sigma_{\max}$ (N/mm^2)
2	6.147	3.266	6.532	3.074
4	5.492	2.083	4.166	2.746
5	1.642	2.511	5.022	0.821
7	0.961	1.879	3.758	0.480
Mean ± SD	3.56 ± 2.64	2.43 ± 0.61	4.87 ± 1.23	1.78 ± 1.32
CV (%)	74.19	25.10	25.26	74.16

Morphological Structure Results

The morphological characteristics of polycaprolactone (PCL)-based biocomposite scaffolds containing a constant amount of hydroxyapatite (8 wt% HA) and varying concentrations of hexagonal boron nitride (hBN) were investigated using field-emission scanning electron microscopy (FEG-SEM). Representative SEM micrographs at different magnifications and the corresponding fiber diameter distributions are presented in Figures 3 and 4. The analysis revealed notable differences in fiber morphology, diameter distribution, and overall structural organization depending on the hBN content. The hBN-free PCL/HA scaffold (0 wt% hBN) exhibited a randomly oriented fibrous network with interconnected fibers and a porous structure. Although the overall fibrous architecture was preserved, local variations in fiber arrangement and pore distribution were observed. The fiber diameter distribution showed a relatively broad range, with an average diameter of 323 ± 175 nm, indicating moderate heterogeneity within the nanofibrous network.

The incorporation of a low hBN concentration (0.05 wt%) resulted in a more refined fibrous morphology while maintaining the porous structure. The fibers appeared thinner and more uniformly distributed compared to the hBN-free scaffold, with an average fiber diameter of 265 ± 155 nm. Despite the overall improvement in fiber uniformity, localized irregularities in fiber arrangement were still observed. A further increase in hBN content to 0.5 wt% led to a more homogeneous and interconnected nanofibrous structure. The fiber network appeared more uniformly distributed, and the variability in fiber diameter was reduced, yielding an average diameter of 265 ± 116 nm. The porous architecture was well preserved, and the scaffold exhibited a more consistent fibrous organization across the examined regions.

In contrast, scaffolds containing 2.5 wt% hBN showed a pronounced change in fiber morphology. The fibrous structure became more heterogeneous, characterized by the presence of thicker fibers and locally dense regions. The fiber diameter distribution shifted toward higher

values, with an average diameter of 604 ± 292 nm, indicating increased fiber thickening and variability. Although the porous structure was still present, the overall uniformity of the fibrous network was reduced at this higher hBN concentration.

Quantitative analysis of FEG-SEM images revealed differences in the apparent two-dimensional (2D) void area fraction among the scaffold formulations. While the PCL/HA scaffold without hBN exhibited a value of 32.04%, the highest value (45.84%) was observed in the group containing 0.05% hBN. The apparent 2D void area fraction decreased to 39.96% and 29.97% in the groups containing 0.5% and 2.5% hBN, respectively. These results indicate that a non-linear change in the apparent 2D void area fraction occurs as the hBN concentration increases.

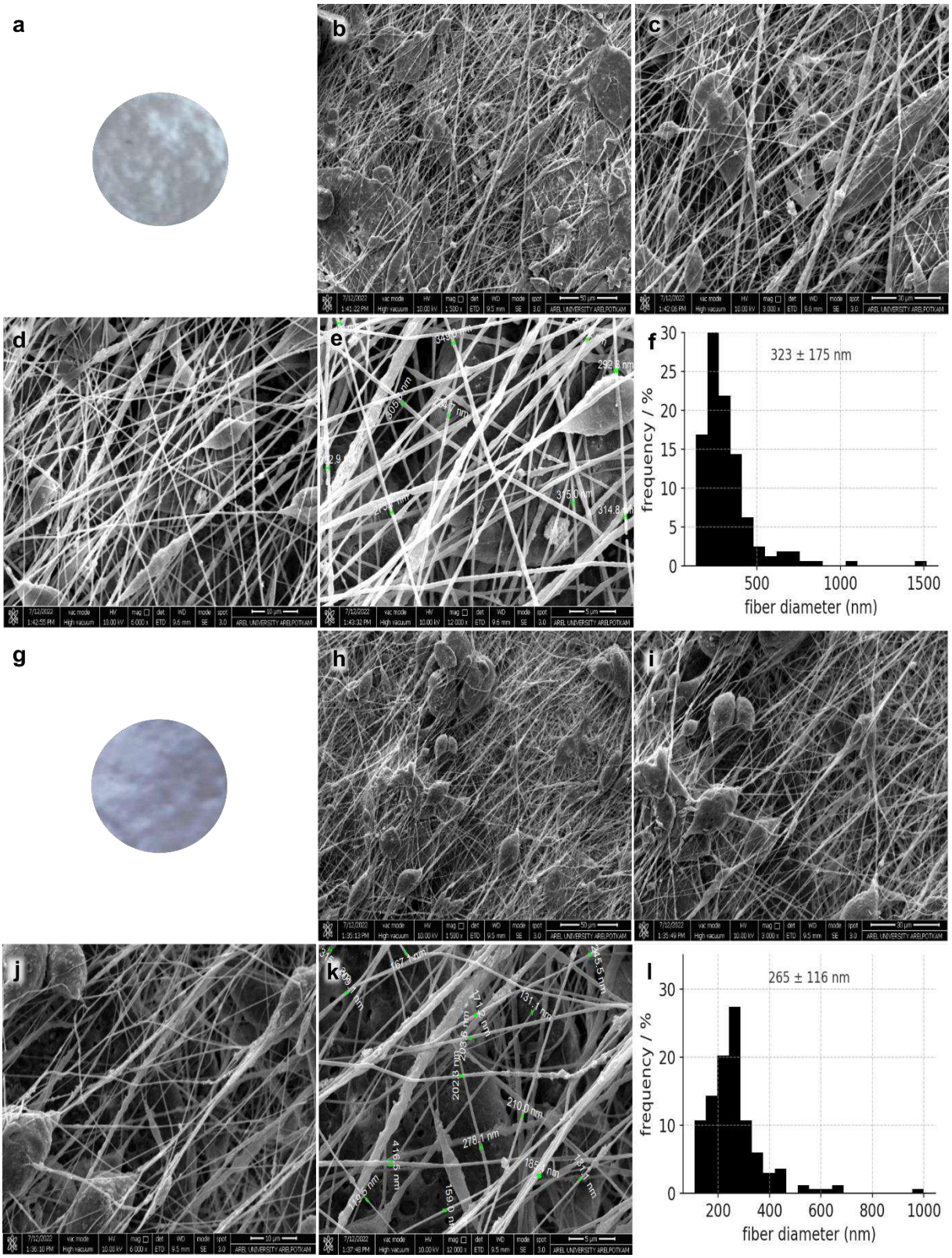


Fig. 3 Morphological characterization and fiber diameter distribution of electrospin PCL–HA-based scaffolds without hBN and with 0.05% hBN incorporation. (a) Representative macroscopic (camera) image of the electrospin PCL–HA scaffold without hBN (0 hBN). (b–e) FEG-SEM micrographs of the 0 hBN scaffold at increasing magnifications: (b) 1500×, (c) 3000×, (d) 6000×, and (e) 12,000×, revealing a randomly oriented fibrous network with interconnected pores and uniform fiber morphology. (f) Fiber diameter distribution histogram of the 0 hBN scaffold, showing an average fiber diameter of 323 ± 175 nm (n = 150). (g) Representative macroscopic (camera) image of the electrospin PCL–HA scaffold containing 0.05% hBN. (h–k)

FEG-SEM micrographs of the 0.05% hBN scaffold at different magnifications: (h) 1500×, (i) 3000×, (j) 6000×, and (k) 12,000×, demonstrating a preserved fibrous architecture with finer fibers and homogeneous morphology following hBN incorporation. (l) Fiber diameter distribution histogram of the 0.05% hBN scaffold, indicating a reduced average fiber diameter of 265 ± 116 nm ($n = 150$).

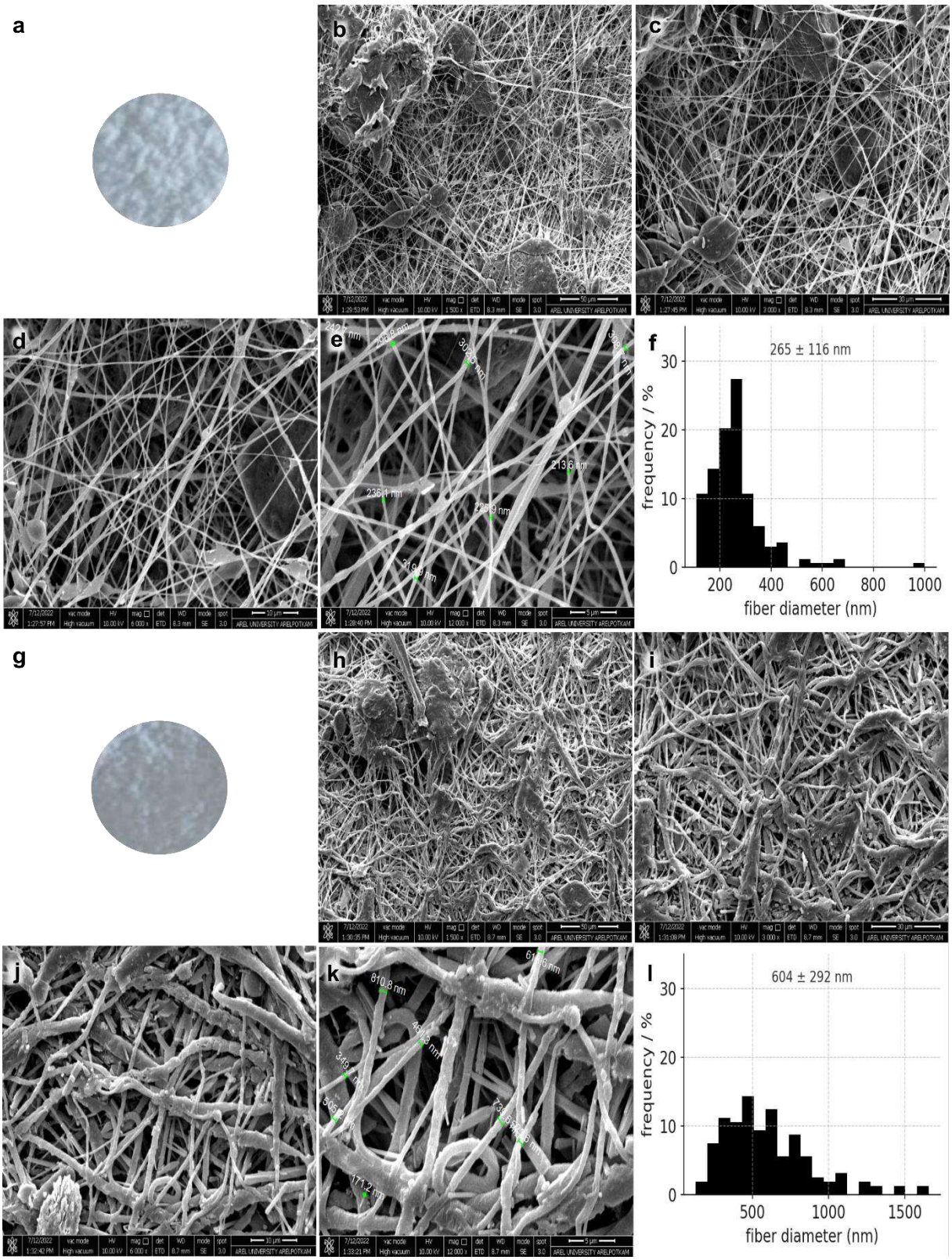


Fig. 4 Morphological characterization and fiber diameter distribution of electrospin PCL–HA-based scaffolds containing 0.5% and 2.5% hBN. (a) Representative macroscopic (camera) image of the electrospin PCL–HA

scaffold containing 0.5% hBN. (b–e) FEG-SEM micrographs of the 0.5% hBN scaffold at increasing magnifications: (b) 1500×, (c) 3000×, (d) 6000×, and (e) 12,000×, revealing a randomly oriented fibrous network with interconnected pores and uniform fiber morphology. (f) Fiber diameter distribution histogram of the 0.5% hBN scaffold, showing an average fiber diameter of 265 ± 116 nm ($n = 150$). (g) Representative macroscopic (camera) image of the electrospin PCL–HA scaffold containing 2.5% hBN. (h–k) FEG-SEM micrographs of the 2.5% hBN scaffold at different magnifications: (h) 1500×, (i) 3000×, (j) 6000×, and (k) 12,000×, demonstrating a preserved fibrous architecture with thicker fibers and homogeneous morphology following increased hBN incorporation. (l) Fiber diameter distribution histogram of the 2.5% hBN scaffold, indicating an increased average fiber diameter of 604 ± 292 nm ($n = 150$).

MTT Analysis Results of Scaffolds

The cytocompatibility of PCL–HA biocomposite scaffolds containing different concentrations of hexagonal boron nitride (hBN) was quantitatively assessed by MTT assay at 24 h and 5 days, with cell viability values normalized to the positive control (Figure 5). All experimental groups exhibited high cell viability at both time points, indicating the absence of acute or delayed cytotoxic effects associated with hBN incorporation.

At 24 h, cell viability remained above 90% across all scaffold groups. The PCL–HA scaffold without hBN showed a slight reduction in viability compared to the positive control; however, this decrease was marginal. Scaffolds containing 0.05% and 0.5% hBN demonstrated moderately lower viability values relative to the control group, while remaining within the range generally accepted as cytocompatible. Notably, the 2.5% hBN containing scaffold exhibited cell viability comparable to the positive control, suggesting that higher hBN content did not adversely affect early cellular metabolic activity.

After 5 days of culture, cell viability was largely preserved in all groups. While the 0.05% and 0.5% hBN groups showed a slight decrease in viability compared to day 1, the 2.5% hBN scaffold demonstrated an apparent increase in metabolic activity, approaching or exceeding the levels observed at earlier time points. This observation suggests a potential time-dependent adaptation of cells to higher hBN content, possibly associated with improved cell–scaffold interactions during prolonged culture.

Statistical analysis revealed no significant differences in cell viability among the scaffold groups at either 24 h or 5 days (one-way ANOVA, $p>0.05$). Nevertheless, a time-dependent trend towards increased metabolic activity was observed, particularly in the 2.5% hBN group at day 5. Although this trend did not reach statistical significance, it indicates that higher hBN concentrations may support sustained cellular metabolic activity over time.

Overall, these findings confirm that the incorporation of hBN into PCL–HA scaffolds does not compromise cytocompatibility and that higher hBN content may offer favorable conditions for long-term cell viability. The relatively large standard deviations observed in some groups suggest biological variability in cell response, emphasizing the need for further investigation using complementary assays and longer culture periods to elucidate the underlying mechanisms of cell–material interactions.

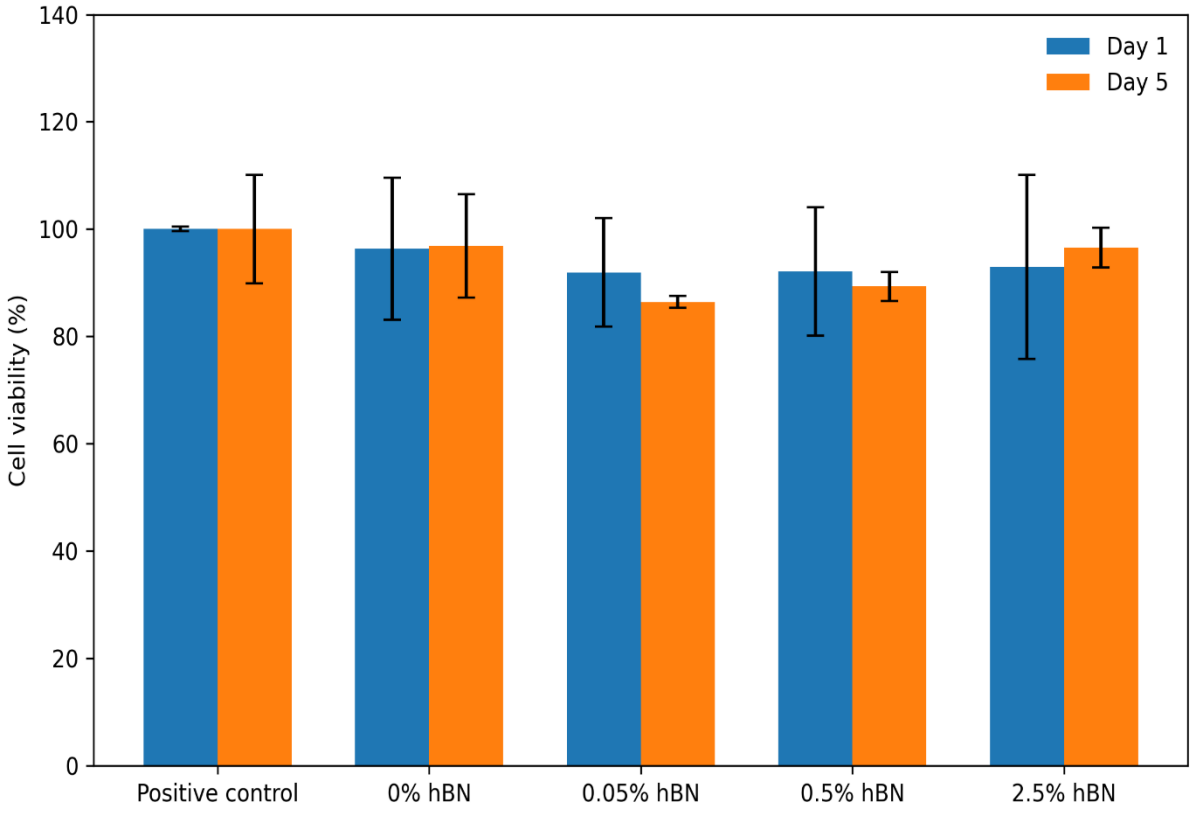


Fig. 5 Cytocompatibility of PCL–HA–hBN scaffolds. Cytocompatibility of PCL–HA biocomposite scaffolds containing different concentrations of hexagonal boron nitride (hBN) evaluated by MTT assay after 24 h (Day 1) and 5 days (Day 5) of rMSC culture. Cell viability was normalized to the positive control (100%). Data are presented as mean ± SD ($n = 3$). No statistically significant differences were observed among the groups at either time point (one-way ANOVA, $p > 0.05$).

Confocal Microscope Images of Scaffold–Cell Structures

In this study, the morphology and spatial distribution of rat mesenchymal stem cells (MSCs) cultured on 10% PCL–8% HA electrospin scaffolds containing different concentrations of hexagonal boron nitride (hBN) were evaluated by fluorescence microscopy using Alexa Fluor® 488–conjugated phalloidin staining. Analyses were performed at two incubation times (day 1 and day 5) and at two magnifications (2.5× and 10×). The green fluorescence signal corresponds to F-actin organization and reflects the distribution of viable cells attached to the scaffold surface.

At day 1 (2.5× and 10×) (Figure 6), cells in the 10% PCL–8% HA scaffold without hBN (control group) exhibited clear initial attachment to the porous nanofibrous structure, with relatively higher overall fluorescence intensity compared to hBN-containing groups. Quantitative ImageJ analysis of mean gray values confirmed that the control group displayed significantly higher fluorescence intensity than the 0.05%, 0.5%, and 2.5% hBN groups ($p<0.05$) (Figure 8).

In scaffolds containing 0.05% hBN, cells were distributed across the scaffold surface; however, the overall fluorescence intensity was significantly lower than that of the control, indicating reduced early cytoskeletal signal intensity. The 0.5% and 2.5% hBN groups showed intermediate fluorescence levels, which were not significantly different from each other but remained lower than the control group. These findings indicate that hBN incorporation, particularly at lower concentrations, slightly reduced early F-actin–associated fluorescence intensity during the initial adhesion phase.

By day 5 (2.5× and 10×) (Figure 7), all scaffold groups exhibited a marked increase in fluorescence intensity and surface coverage compared to day 1, indicating progressive cell spreading and increased cytoskeletal organization over time. The control group maintained the highest mean fluorescence intensity among all groups. Scaffolds containing 0.05% and 0.5% hBN showed significantly lower fluorescence intensity compared to the control ($p<0.05$), while

no statistically significant difference was observed between the control and the 2.5% hBN group ($p>0.05$) (Figure 8).

Among the hBN-containing scaffolds, the 2.5% hBN group exhibited the highest fluorescence intensity at day 5, suggesting improved cellular adaptation over time at higher hBN content. Results supported a concentration- and time-dependent cellular response to hBN incorporation. While early-stage cytoskeletal fluorescence was reduced in hBN-containing scaffolds compared to the control, prolonged culture led to increased fluorescence intensity across all groups, with the 2.5% hBN scaffold approaching control levels at day 5. These observations are consistent with the quantitative ImageJ fluorescence analysis and indicate that hBN does not impair long-term cell attachment or cytoskeletal development within the investigated.

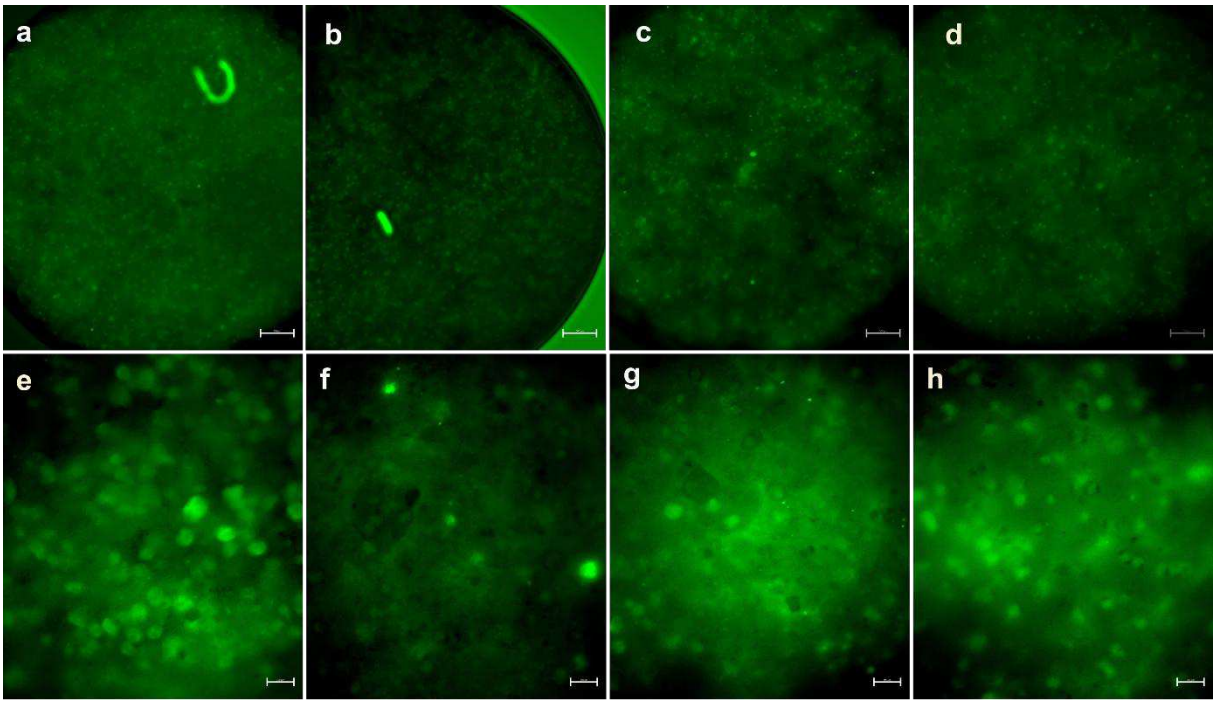


Fig. 6 Fluorescence microscopy images of rMSCs cultured on PCL–HA–hBN scaffolds at day 1. Fluorescence microscopy images of rat mesenchymal stem cells (rMSCs) cultured on 10% PCL–8% HA electrospin scaffolds containing different concentrations of hexagonal boron nitride (hBN) and stained with Alexa Fluor® 488–conjugated phalloidin. (a–d) Low-magnification images (2.5×, scale bar: 500 µm) of scaffolds containing (a) 0 hBN, (b) 0.05% hBN, (c) 0.5% hBN, and (d) 2.5% hBN. (e–h) Higher-magnification images (10×) of the corresponding groups: (e) 0 hBN, (f) 0.05% hBN, (g) 0.5% hBN, and (h) 2.5% hBN. Green fluorescence indicates F-actin organization and reflects the distribution of viable cells on the scaffold surface.

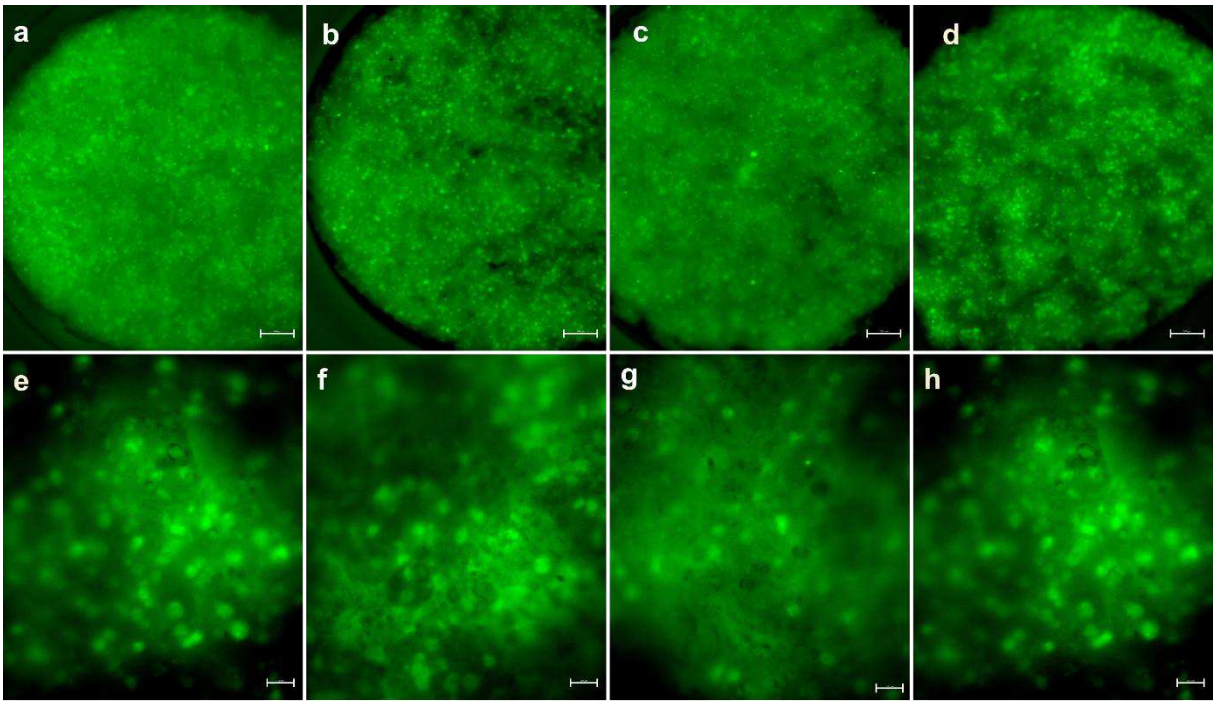


Fig. 7 Fluorescence microscopy images of rMSCs cultured on PCL–HA–hBN scaffolds at day 5. (a–d) Low-magnification images (2.5×, scale bar: 500 μm) of scaffolds containing (a) 0 hBN, (b) 0.05% hBN, (c) 0.5% hBN, and (d) 2.5% hBN. (e–h) Higher-magnification images (10×) of the corresponding groups: (e) 0 hBN, (f) 0.05% hBN, (g) 0.5% hBN, and (h) 2.5% hBN.

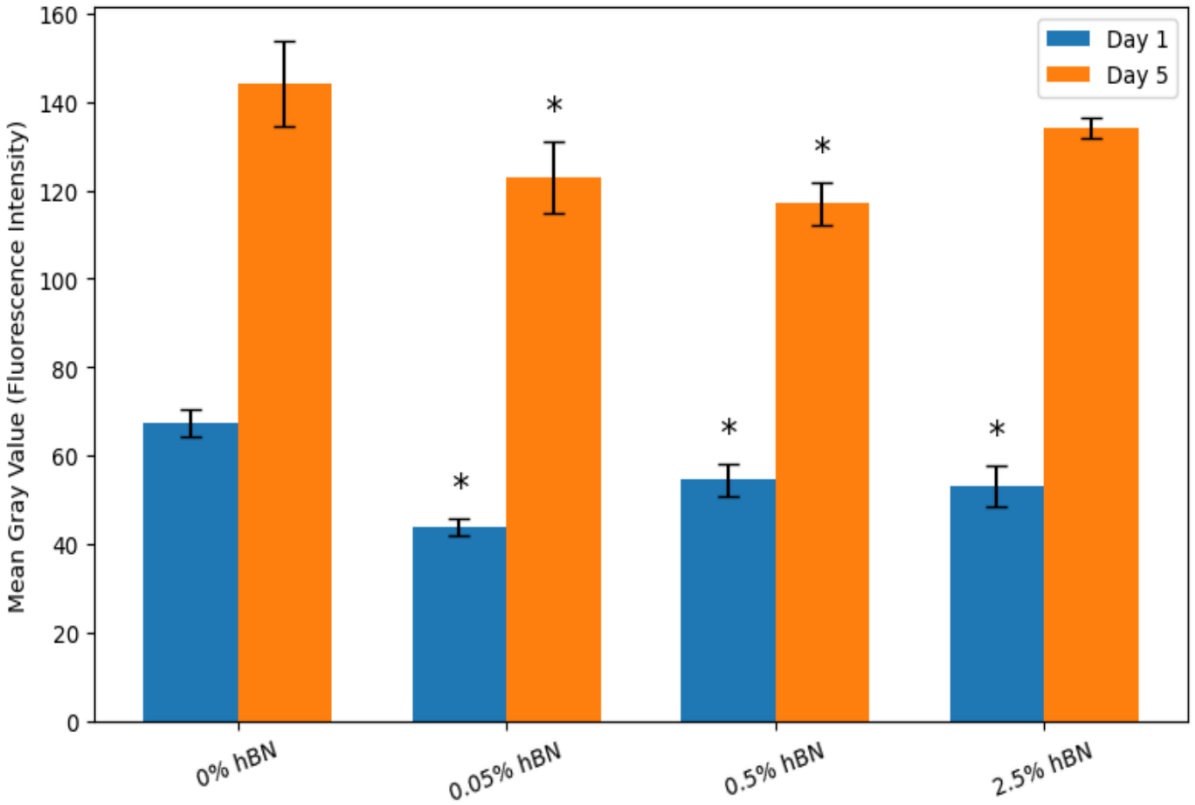


Fig. 8 Quantitative analysis of F-actin fluorescence intensity (mean gray value) obtained from CLSM images at day 1 and day 5. Data are presented as mean ± SD (n = 3). Statistical analysis was performed using one-way ANOVA followed by Tukey's post-hoc test. Asterisks indicate statistically significant differences compared to the control group (0% hBN): *$p < 0.05$.

Alizarin Red Images of Scaffold–Cell Structures

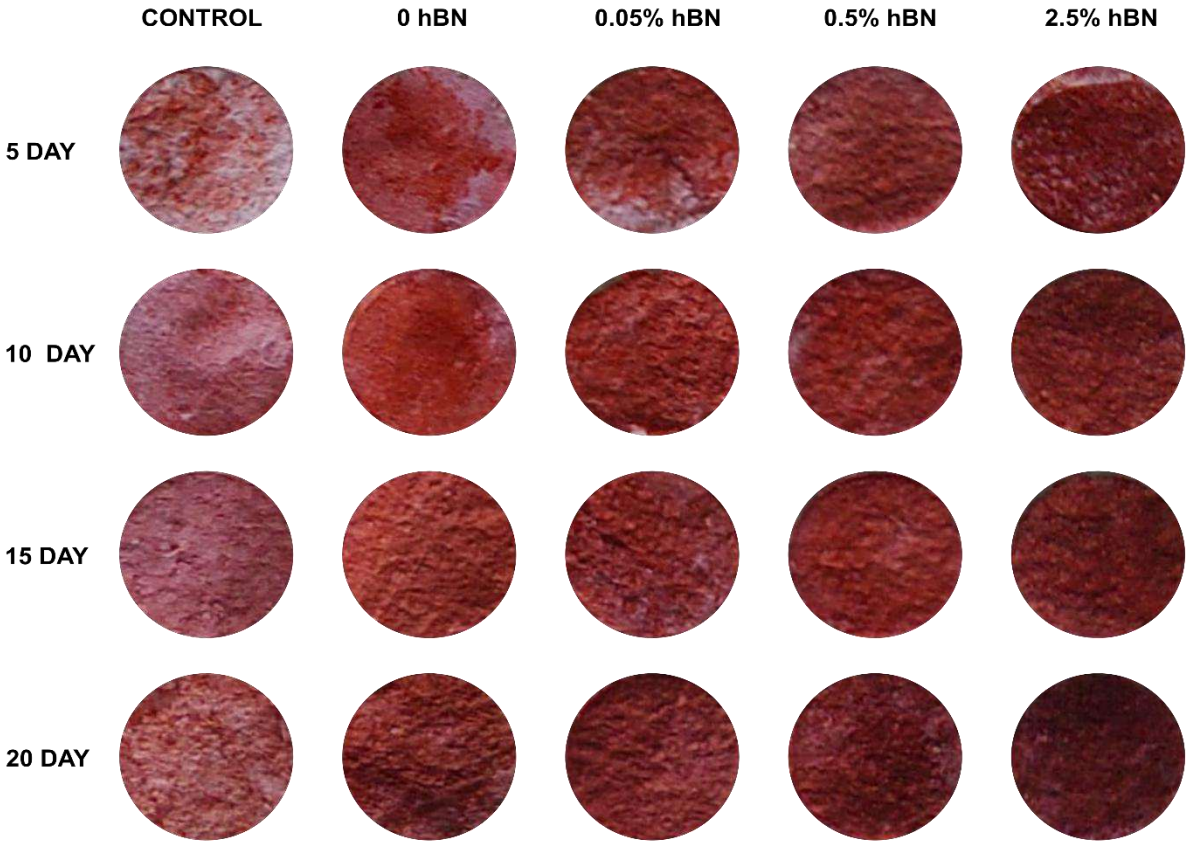
The osteogenic differentiation and mineralized matrix formation of rat mesenchymal stem cells (MSCs) cultured on electrospin PCL–HA and hBN-doped biocomposite scaffolds were evaluated by Alizarin Red S staining at days 5, 10, 15, and 20. Quantitative analysis of mineralized areas was performed using ImageJ software, and the percentage of Alizarin Red–positive area was calculated under identical imaging and thresholding conditions (Figures 9–10).

At day 5, quantitative analysis revealed that mineral deposition was at an early stage in all experimental groups (Figure 9, Day 5). The control group exhibited minimal Alizarin Red–positive area, confirming the absence of osteogenic induction. Scaffolds containing PCL–HA without hBN showed a slight but significant increase in mineralized area compared to the control ($p<0.05$). Notably, scaffolds containing 0.05% and 0.5% hBN demonstrated a statistically significant increase in Alizarin Red–positive area relative to the control ($p<0.01$ and $p<0.001$, respectively), indicating an early stimulatory effect of low-to-moderate hBN concentrations on osteogenic mineralization. In contrast, the 2.5% hBN group showed the highest mineralized area at this time point, with a highly significant increase compared to the control ($p<0.001$).

By day 10, a pronounced progression in osteogenic differentiation was observed across all scaffold groups (Figure 9, Day 10). Quantitative results demonstrated a significant increase in mineralized area in all hBN-containing scaffolds compared to the control ($p<0.05$ to $p<0.001$). The 0.05% and 0.5% hBN groups exhibited markedly higher Alizarin Red–positive areas than the PCL–HA group, suggesting enhanced matrix mineralization at intermediate hBN concentrations. Although the 2.5% hBN group also showed significantly increased mineralization relative to the control, its mean mineralized area remained comparable to, or slightly lower than, the 0.5% hBN group at this time point.

At day 15, mineral deposition increased substantially in all experimental groups, reflecting advanced osteogenic differentiation (Figure 9, Day 15). Quantitative analysis indicated that scaffolds containing 0.5% hBN exhibited the highest percentage of Alizarin Red–positive area, significantly exceeding the control and PCL–HA groups ($p<0.001$). The 0.05% hBN group also demonstrated a strong mineralization response, while the 2.5% hBN group showed a comparatively lower, yet still significant, increase in mineralized area relative to the control ($p<0.01$). These findings suggest that moderate hBN concentrations are particularly effective in promoting osteogenic matrix formation at intermediate culture durations.

By day 20, osteogenic differentiation approached completion, with extensive mineralized matrix formation observed in all scaffold groups (Figure 9, Day 20). Quantitative ImageJ analysis revealed that all hBN-containing scaffolds exhibited significantly higher Alizarin Red–positive areas compared to the control ($p<0.001$). Among the experimental groups, the 2.5% hBN scaffolds displayed the highest mineralized area at this late time point, followed closely by the 0.5% and 0.05% hBN groups. The PCL–HA scaffold without hBN also showed substantial mineralization but remained significantly lower than the hBN-doped groups.



554

555 **Fig. 9** Alizarin Red S staining of rMSCs cultured on PCL–HA–hBN scaffolds. Representative images showing
556 calcium deposition by rat mesenchymal stem cells (rMSCs) cultured on 10% PCL–8% HA electrospin scaffolds
557 containing different concentrations of hexagonal boron nitride (hBN). Images illustrate mineralized matrix
558 formation on scaffolds with varying hBN content. Red staining intensity indicates calcium-rich deposits associated
559 with osteogenic differentiation.

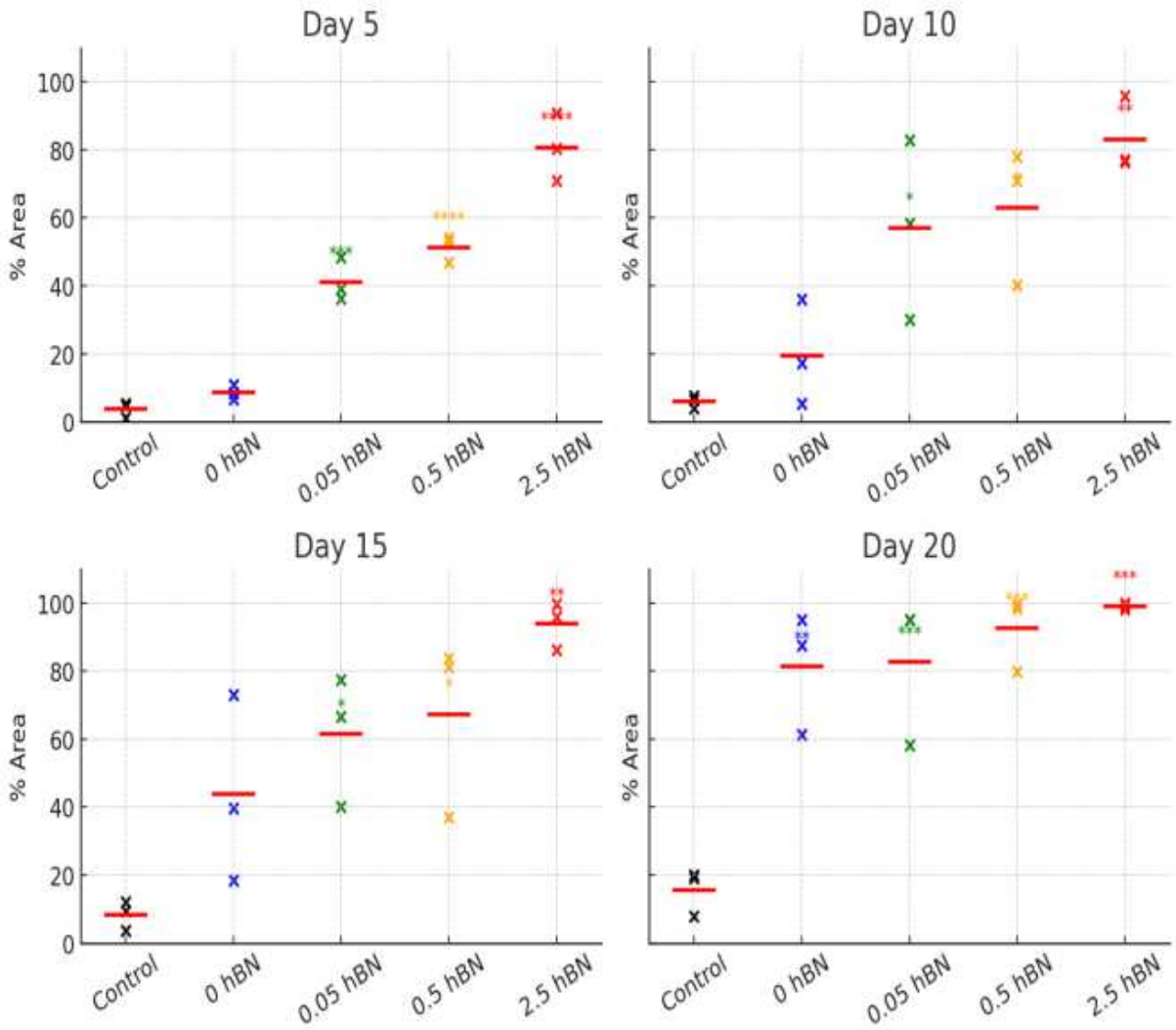


Fig. 10 Quantitative analysis of mineralized area on PCL–HA–hBN scaffolds over time. Quantitative analysis of Alizarin Red S–stained mineralized area (%) of rat mesenchymal stem cells (rMSCs) cultured on 10% PCL–8% HA electrospin scaffolds containing different concentrations of hexagonal boron nitride (hBN) at day 5, day 10, day 15, and day 20. Data points represent individual measurements, and horizontal bars indicate mean values. Mineralized area increased over time in all scaffold groups, with hBN-containing scaffolds showing enhanced mineral deposition at later time points. Statistical significance was determined using appropriate statistical tests (*$p < 0.05$, **$p < 0.01$, ***$p < 0.001$).

DISCUSSION

Bone injury represents one of the most common traumatic conditions, and the healing process remains particularly challenging in cases involving large bone defects or systemic disorders such as osteoporosis. In recent years, bone tissue engineering has emerged as a promising strategy that integrates biomaterials, cells, and bioactive cues to accelerate bone regeneration, enhance cellular proliferation, and provide mechanical stability at the defect site [39]. In this context, electrospin nanofiber scaffolds produced from biocompatible and biodegradable polymers have become a major focus of attention due to their ability to mimic the extracellular matrix by providing a suitable microenvironment for cell attachment and osteogenic differentiation [40]. In this study, nanofiber scaffolds containing polycaprolactone (PCL), hydroxyapatite (HA) and varying concentrations of hexagonal boron nitride (hBN) were successfully produced by electrospinning technique; Their structural, morphological, mechanical and biological properties have been systematically characterized. Additionally, in order to evaluate the cellular compatibility and osteogenic mineralization potential of these scaffolds, their interactions with rat mesenchymal stem cells (MSCs) were examined, and preliminary findings regarding their potential in bone tissue engineering applications were obtained. supported the incorporation of PCL, HA, and hBN into the nanofibrous scaffolds. Consistent with previous studies, characteristic PCL bands corresponding to asymmetric and symmetric CH2 stretching and carbonyl (C=O) vibrations were observed [41]. In agreement with the findings of Aki et al., the presence of hBN was confirmed by the appearance of bands in the region of ~1237 cm^{-1} and ~742 cm^{-1} [40]. Importantly, variations in the intensity and position of the carbonyl (C=O) and PO_4^{-3} bands with increasing hBN concentration suggest chemical interactions between hBN and the polymer matrix, as well as surface interactions with HA particles. These results indicate that hBN was not merely physically embedded but was

effectively integrated into the composite scaffold structure, in line with previously reported polymer ceramic boron systems.

Morphological analysis conducted via FEG-SEM revealed that the addition of hBN influences fiber morphology, diameter distribution, and structural arrangement. Consistent with the observations reported by Özbek et al. interconnected fiber networks were observed across all scaffold groups; however, the morphological characteristics of these networks varied depending on the hBN concentration [42]. The incorporation of 0.05% and 0.5% hBN resulted in the formation of finer fibers and a relatively more uniform fiber distribution compared to the scaffold structure without hBN. In contrast, the group containing 2.5% hBN exhibited thicker fibers, greater morphological heterogeneity, and more pronounced localized agglomerations, which could negatively affect mechanical integrity. FEG-SEM image analysis revealed higher visible void area fractions at hBN concentrations of 0.05% and 0.5%, whereas a lower value was observed at 2.5% hBN; this may be associated with fiber aggregation and particle clustering. Although further analysis is required to evaluate three-dimensional porosity, these morphological differences could influence cell adhesion and nutrient transport. Mechanical tests have further elucidated the impact of hBN concentration on scaffold performance. While the PCL/HA scaffold without hBN exhibited the highest tensile strength (3.074 MPa), the addition of 0.05% hBN resulted in a slight decrease to 2.746 MPa. Further increases in hBN concentration led to a marked reduction in tensile strength, with values dropping to 0.821 MPa and 0.480 MPa at hBN concentrations of 0.5% and 2.5%, respectively. This decline may be attributed to the increased fiber heterogeneity and particle agglomeration observed in the SEM images, which can negatively affect stress distribution within the fibrous network. Cell viability and proliferation were assessed using the MTT assay, revealing time-dependent cellular responses to hBN incorporation. Day 1 results indicated a slight reduction in cell viability in scaffolds containing higher hBN concentrations, suggesting a possible early inhibitory effect

on cellular metabolic activity. This effect may be attributed to changes in surface charge, ion balance at the cell membrane, and alterations in surface topography that can transiently limit cell adhesion [42, 43]. However, by day 5, cell viability increased across all groups, indicating cellular adaptation to the scaffold environment. Importantly, no statistically significant differences in cell viability were observed among the scaffold groups, suggesting that hBN incorporation did not induce substantial cytotoxic effects under the investigated conditions. These findings support the short-term cellular compatibility of the developed scaffolds. The cellular responses to materials containing hBN (hexagonal boron nitride) in bone tissue engineering which vary depending on concentration have been evaluated in various studies. Mayeen et al. reported that MG-63 and HOS cells cultured on electrospin PVDF/HA (polyvinylidene fluoride/hydroxyapatite) nanofiber scaffolds containing 2.5%, 5%, and 10% (by weight) boron nitride nanosheets (BNNS) retained their viability and exhibited positive cellular responses [44]. In contrast, Ensoylu et al. observed 86% viability in MC3T3-E1 osteoblastic cells incubated for 72 hours with borate based bioactive glass scaffolds containing 0.2% (by weight) hBN; however, they found that increasing the hBN content to 0.5% or higher led to an approximately 50% reduction in cell viability [45]. Meanwhile, Kar et al. reported that hBN nanoparticles administered intravenously to rats particularly at doses of 1600 and 3200 μg/kg caused changes associated with oxidative stress, such as the disruption of thiol/disulfide homeostasis, increased lipid peroxidation, and decreased catalase activity [46]. The discrepancies among these studies indicate that the cellular effects of hBN depend not only on the concentration used but also on the physicochemical properties of the nanoparticles, the composition of the scaffold matrix, the degradation behavior of that matrix, and the specific conditions under which exposure occurs.

Fluorescence microscopy analyses revealed concentration-dependent differences in F-actin fluorescence intensity, suggesting that the incorporation of hBN may influence cellular

cytoskeletal organization. On day 1, all groups containing hBN exhibited lower fluorescence intensities compared to the scaffold without hBN. Although fluorescence intensity increased across all groups by day 5, the groups containing 0.05% and 0.5% hBN continued to show significantly lower values than the control group. In contrast, the 2.5% hBN group displayed a smaller difference relative to the control group at this time point. These findings, consistent with the MTT results, suggest that the concentration of hBN can modulate cell-scaffold interactions and cytoskeletal organization without significantly compromising cellular metabolic activity.

Osteogenic mineralization was evaluated on days 5, 10, 15, and 20 using Alizarin Red S staining. The results showed a time-dependent increase in mineralized matrix formation across the scaffold groups, with the highest values generally observed in the 2.5% hBN group, particularly during the early culture period. By day 20, a significant amount of mineralization was observed in the scaffold groups. These findings are consistent with previous studies highlighting the potential of boron-containing biomaterials in bone tissue engineering. Wu et al. reported that the incorporation of boron into bioactive glass scaffolds enhanced osteoblast proliferation and the expression of bone-related genes [43]. Similarly, Yayla et al. demonstrated positive bone healing responses using boron nitride/hydroxyapatite composites in an in vivo rat defect model [47]. Although these studies utilized different material systems and experimental models, their findings support the potential contribution of boron-containing materials to bone-related cellular responses. Accordingly, the present results indicate that the inclusion of hBN can promote the formation of a mineralized matrix within PCL/HA nanofiber scaffolds under osteogenic culture conditions. The effects of hBN addition were investigated by comparing them with a PCL/HA scaffold structure that does not contain hBN, in order to evaluate its mechanical and biological contributions. To place these findings in a broader context, it is important to consider the performance of other nanofiller-reinforced scaffolds reported in the

literature. Previous studies in the literature have shown that the impact of nanofillers on scaffold performance varies depending on the material composition and the specific properties of the filler. Dalgic et al. reported that PCL/SiHA/GO scaffolds produced via electrospinning exhibited increased cell adhesion and proliferation, though no consistent improvement in tensile strength was observed [48]. Marrella et al. demonstrated that PCL nanofibers reinforced with GO and rGO showed improved tensile properties; furthermore, they found that rGO supported cell-mediated mineralization and the expression of osteogenic markers [33]. Similarly, Fu et al. observed enhanced mechanical strength and stronger osteogenic responses in PLGA/HA/GO scaffolds [49]. In contrast, Kashte et al. (2024) noted that there was no significant increase in mineralization for GO-coated PCL scaffolds compared to those coated with graphene [50]. In the present study, it was determined that higher hBN concentrations specifically at a 2.5% ratio promote the formation of a mineralized matrix but also lead to a reduction in tensile strength. Despite differences in scaffold composition and experimental conditions that limit direct comparisons, these findings highlight the importance of optimizing hBN concentration to achieve an appropriate balance between osteogenic potential and mechanical stability.

CONCLUSION

This study demonstrates that hBN-incorporated PCL/HA nanofibrous scaffolds support rat-derived stem cell proliferation and osteogenic differentiation. In particular, scaffolds containing higher amounts of hBN exhibited superior performance in terms of osteogenic differentiation by enhancing cellular proliferation and promoting mineralization associated with osteoblast activity, thereby highlighting their potential as alternative candidates for bone tissue engineering. Furthermore, FEG-SEM based image analysis has revealed variations in the visible void area fraction depending on the hBN concentration, highlighting the importance of scaffold structure (morphology) in biomaterial design. This work constitutes a fundamental study aimed at determining the optimal hBN content required for the fabrication of bone

constructs intended for clinical research applications. However, considering that high hBN concentrations may increase the mechanical brittleness of the scaffolds, future studies should focus on identifying the optimal hBN dosage suitable for load-bearing bone applications. Furthermore, long-term biocompatibility assessments are strongly recommended. In addition, the present findings suggest that such biocomposite scaffolds could be further advanced by integrating drug delivery systems and should be evaluated through in vivo studies for the treatment of bone defects.

DECLARATIONS

Funding: This study was supported by the Scientific Research Projects Unit of Istanbul University (Project No: TYL-2021-37593)

Acknowledgements: We would also like to extend our sincere gratitude to Veterinarian Mert Celikten from the Bezmialem Vakıf University Experimental Application and Research Center for his invaluable assistance with the animal experiments

Ethics approval: The experimental animals used were obtained from Bezmialem Vakıf University Experimental Application and Research Center and the animals were kept under appropriate conditions during the experiment. Ethical rules were followed throughout the study. Permission for animal studies was approved by the Bezmialem Vakıf University Animal Experiments Local Ethics Committee (Ethics Committee No: 2021/251).

Authors' contributions: Gunnaz C: Conceptualization, investigation, methodology and writing original draft, resources, supervision and writing—review & editing ; Erdi B.: Formal analysis, Investigation, resources, methodology data curation and writing—review & editing; Bukem T.: Validation, Formal analysis, resources and methodology; Gurcan A.: Formal analysis, methodology and ethical permission; Leyla T S: Methodology, writing—review & editing; Isıl A.: Conceptualization, methodology, investigation, resources, supervision and writing- review & editing and project administration. **The authors declare no conflict of interest.**

REFERANCE

1. Emara, K.M., R.A. Diab, and A.K. Emara, *Recent biological trends in management of fracture non-union.* World J Orthop, 2015. 6(8): p. 623-8.
2. Lei, T., et al., *Silicon-incorporated nanohydroxyapatite-reinforced poly(ε-caprolactone) film to enhance osteogenesis for bone tissue engineering applications.* Colloids and Surfaces B: Biointerfaces, 2020. 187: p. 110714.
3. Wang, W. and K.W.K. Yeung, *Bone grafts and biomaterials substitutes for bone defect repair: A review.* Bioactive Materials, 2017. 2(4): p. 224-247.
4. Doğan, A., et al., *Boron containing poly-(lactide-co-glycolide) (PLGA) scaffolds for bone tissue engineering.* Materials Science and Engineering: C, 2014. 44: p. 246-253.
5. Al-Tamimi, A.A., et al., *Metallic bone fixation implants: a novel design approach for reducing the stress shielding phenomenon.* Virtual and Physical Prototyping, 2017. 12(2): p. 141-151.
6. Bandyopadhyay, A., et al., *Improving biocompatibility for next generation of metallic implants.* Progress in Materials Science, 2023. 133: p. 101053.
7. Dejob, L., et al., *Electrospinning of in situ synthesized silica-based and calcium phosphate bioceramics for applications in bone tissue engineering: A review.* Acta Biomater, 2021. 123: p. 123-153.
8. Catledge, S.A., et al., *An electrospun triphasic nanofibrous scaffold for bone tissue engineering.* Biomed Mater, 2007. 2(2): p. 142-50.
9. Park, H., et al., *Nanofibrous mineralized electrospun scaffold as a substrate for bone tissue regeneration.* Journal of Biomedical Nanotechnology, 2016. 12(11): p. 2076-2082.
10. Safari, B., et al., *Osteogenic effects of the bioactive small molecules and minerals in the scaffold-based bone tissue engineering.* Colloids and Surfaces B: Biointerfaces, 2021. 198: p. 111462.
11. Dwivedi, R., et al., *Polycaprolactone as biomaterial for bone scaffolds: Review of literature.* Journal of Oral Biology and Craniofacial Research, 2020. 10(1): p. 381-388.
12. Qi, H., et al., *Bioactivity assessment of PLLA/PCL/HAP electrospun nanofibrous scaffolds for bone tissue engineering.* Life Sciences, 2016. 148: p. 139-144.
13. Turnbull, G., et al., *3D bioactive composite scaffolds for bone tissue engineering.* Bioact Mater, 2018. 3(3): p. 278-314.
14. Samavedi, S., A.R. Whittington, and A.S. Goldstein, *Calcium phosphate ceramics in bone tissue engineering: A review of properties and their influence on cell behavior.* Acta Biomaterialia, 2013. 9(9): p. 8037-8045.
15. Murugan, S. and S.R. Parcha, *Fabrication techniques involved in developing the composite scaffolds PCL/HA nanoparticles for bone tissue engineering applications.* J Mater Sci Mater Med, 2021. 32(8): p. 93.
16. Shi, H., et al., *Hydroxyapatite Based Materials for Bone Tissue Engineering: A Brief and Comprehensive Introduction.* Crystals, 2021. 11(2): p. 149.
17. Ciftci, E., et al., *Boron Containing Nano Hydroxyapatites (B-n-HAp) Stimulate Mesenchymal Stem Cell Adhesion, Proliferation and Differentiation*. Vol. 631. 2014.
18. Nielsen, F.H., *Is boron nutritionally relevant?* Nutr Rev, 2008. 66(4): p. 183-91.
19. Ying, X., et al., *Effect of boron on osteogenic differentiation of human bone marrow stromal cells.* Biol Trace Elem Res, 2011. 144(1-3): p. 306-15.
20. Hakki, S.S., B.S. Bozkurt, and E.E. Hakki, *Boron regulates mineralized tissue-associated proteins in osteoblasts (MC3T3-E1).* J Trace Elem Med Biol, 2010. 24(4): p. 243-50.
21. Pizzorno, L., *Nothing Boring About Boron.* Integr Med (Encinitas), 2015. 14(4): p. 35-48.

22. Rondanelli, M., et al., *Pivotal role of boron supplementation on bone health: A narrative review.* Journal of Trace Elements in Medicine and Biology, 2020. 62: p. 126577.
23. Eseceli, H., T. Onay, and B. Gönen, *Bor'un İnsan Sağlığı ve Beslenme Üzerine Etkisi.* SDÜ SAĞLIK BİLİMLERİ DERGİSİ, 2018. 9: p. 119-122.
24. Routray, I. and S. Ali, *Boron Induces Lymphocyte Proliferation and Modulates the Priming Effects of Lipopolysaccharide on Macrophages.* PLOS ONE, 2016. 11(3): p. e0150607.
25. Karabal, E., M. Yücel, and H.A. Öktem, *Antioxidant responses of tolerant and sensitive barley cultivars to boron toxicity.* Plant Science, 2003. 164(6): p. 925-933.
26. DeLeo, P.C., et al., *Assessment of consumer exposure to boron in cleaning products: a case study of Canada.* Crit Rev Toxicol, 2021. 51(4): p. 359-371.
27. Doğan, D., et al., *Boron nitride decorated poly(vinyl alcohol)/poly(acrylic acid) composite nanofibers: A promising material for biomedical applications.* Journal of the Mechanical Behavior of Biomedical Materials, 2023. 141: p. 105773.
28. Hiew, V.V., S.F.B. Simat, and P.L. Teoh, *The Advancement of Biomaterials in Regulating Stem Cell Fate.* Stem Cell Rev Rep, 2018. 14(1): p. 43-57.
29. Nair, A. and L. Tang, *Influence of scaffold design on host immune and stem cell responses.* Seminars in Immunology, 2017. 29: p. 62-71.
30. Undale, A.H., et al., *Mesenchymal stem cells for bone repair and metabolic bone diseases.* Mayo Clin Proc, 2009. 84(10): p. 893-902.
31. Atila, A., et al., *Study of the boron levels in serum after implantation of different ratios nano-hexagonal boron nitride–hydroxy apatite in rat femurs.* Materials Science and Engineering: C, 2016. 58: p. 1082-1089.
32. Buluş, E., et al., *Production and Characterization of Natural Sourced Hydroxyapatite Added Polystyrene Tissue Scaffolds by Electrospinning.* JOURNAL OF MATERIALS AND ELECTRONIC DEVICES, 2020. 6(1): p. 12-18.
33. Marrella, A., et al., *"Green-reduced" graphene oxide induces in vitro an enhanced biomimetic mineralization of polycaprolactone electrospun meshes.* Mater Sci Eng C Mater Biol Appl, 2018. 93: p. 1044-1053.
34. Gnecchi, M. and L.G. Melo, *Bone marrow-derived mesenchymal stem cells: isolation, expansion, characterization, viral transduction, and production of conditioned medium.* Methods Mol Biol, 2009. 482: p. 281-94.
35. Padash, A., et al., *Osteogenic differentiation of mesenchymal stem cells on the bimodal polymer polyurethane/polyacrylonitrile containing cellulose phosphate nanowhisker.* Hum Cell, 2021. 34(2): p. 310-324.
36. Fang, R., et al., *Electrospun PCL/PLA/HA based nanofibers as scaffold for osteoblast-like cells.* J Nanosci Nanotechnol, 2010. 10(11): p. 7747-51.
37. Litvinov, D. and R. Clarke, *Reduced bias growth of pure-phase cubic boron nitride.* Applied physics letters, 1997. 71(14): p. 1969-1971.
38. Xue, J., et al., *Electrospinning and Electrospun Nanofibers: Methods, Materials, and Applications.* Chem Rev, 2019. 119(8): p. 5298-5415.
39. Ho-Shui-Ling, A., et al., *Bone regeneration strategies: Engineered scaffolds, bioactive molecules and stem cells current stage and future perspectives.* Biomaterials, 2018. 180: p. 143-162.
40. Aki, D., et al., *3D printing of PVA/hexagonal boron nitride/bacterial cellulose composite scaffolds for bone tissue engineering.* Materials & Design, 2020. 196: p. 109094.
41. Liu, S., et al., *Current applications of poly(lactic acid) composites in tissue engineering and drug delivery.* Composites Part B: Engineering, 2020. 199: p. 108238.

42. Ozbek, B., et al., *Production of the novel fibrous structure of poly(ε-caprolactone)/tri-calcium phosphate/hexagonal boron nitride composites for bone tissue engineering.* Journal of the Australian Ceramic Society, 2017. 54.
43. Wu, C., et al., *Proliferation, differentiation and gene expression of osteoblasts in boron-containing associated with dexamethasone deliver from mesoporous bioactive glass scaffolds.* Biomaterials, 2011. 32(29): p. 7068-7078.
44. Mayeen, A., et al., *Flexible, electrospun boron nitride nanosheets (BNNS)/hydroxyapatite –PVDF nanofibers with superior piezoelectric/ferroelectric, biocompatible features for effective bone tissue regeneration.* Journal of Alloys and Compounds, 2024. 1002: p. 175111.
45. Ensoylu, M., A.M. Deliormanlı, and H. Atmaca, *Preparation, Characterization, and Drug Delivery of Hexagonal Boron Nitride-Borate Bioactive Glass Biomimetic Scaffolds for Bone Tissue Engineering.* Biomimetics (Basel), 2022. 8(1).
46. Kar, F., et al., *Hexagonal boron nitride nanoparticles trigger oxidative stress by modulating thiol/disulfide homeostasis.* Human & Experimental Toxicology, 2021. 40(9): p. 1572-1583.
47. Yayla, M., et al., *Regenerative Effect of Resorbable Scaffold Embedded Boron-Nitride/Hydroxyapatite Nanoparticles in Rat Parietal Bone.* J Nanosci Nanotechnol, 2020. 20(2): p. 680-691.
48. Dalgic, A.D., et al., *Silicate-doped nano-hydroxyapatite/graphene oxide composite reinforced fibrous scaffolds for bone tissue engineering.* J Biomater Appl, 2018. 32(10): p. 1392-1405.
49. Fu, C., et al., *Enhanced cell proliferation and osteogenic differentiation in electrospun PLGA/hydroxyapatite nanofibre scaffolds incorporated with graphene oxide.* PLoS One, 2017. 12(11): p. e0188352.
50. Kashte, S.B., et al., *Osteoinductive potential of graphene and graphene oxide for bone tissue engineering: a comparative study.* J Orthop Surg Res, 2024. 19(1): p. 527.